



Cite this: *RSC Adv.*, 2017, 7, 31027

First-principles study of decomposition mechanisms of $\text{Mg}(\text{BH}_4)_2 \cdot 2\text{NH}_3$ and $\text{LiMg}(\text{BH}_4)_3 \cdot 2\text{NH}_3$

Xiaowei Chen,^a Renquan Li,^a Guanglin Xia,^b Hongsheng He,^a Xiuqing Zhang,^a Weidong Zou^{*a} and Xubin Yu^{*b}

The decomposition mechanisms of $\text{Mg}(\text{BH}_4)_2 \cdot 2\text{NH}_3$ and $\text{LiMg}(\text{BH}_4)_3 \cdot 2\text{NH}_3$ were studied by using density functional theory calculations. Compared to that of $\text{Mg}(\text{BH}_4)_2 \cdot 2\text{NH}_3$, the incorporation of LiBH_4 with the formation of $\text{LiMg}(\text{BH}_4)_3 \cdot 2\text{NH}_3$ slightly increased Bader charges of B atoms, meanwhile it decreased Bader charges of N atoms. $\text{Mg}(\text{BH}_4)_2 \cdot 2\text{NH}_3$ shows a low ammonia vacancy diffusion barrier, but relatively high ammonia vacancy formation energy, which lead to a low concentration of NH_3 vacancies and limit NH_3 transportation. In contrast to that of $\text{Mg}(\text{BH}_4)_2 \cdot 2\text{NH}_3$, $\text{LiMg}(\text{BH}_4)_3 \cdot 2\text{NH}_3$ has a relatively high ammonia vacancy formation energy and diffusion barrier, which suppresses ammonia release. The incorporation of LiBH_4 and $\text{Mg}(\text{BH}_4)_2 \cdot 2\text{NH}_3$ does not decrease but increases the hydrogen formation barrier of $\text{LiMg}(\text{BH}_4)_3 \cdot 2\text{NH}_3$, resulting in a slight increase in the dehydrogenation peak temperature, consistent with experimental results.

Received 11th May 2017

Accepted 6th June 2017

DOI: 10.1039/c7ra05322c

rsc.li/rsc-advances

Introduction

Recently, many efforts have been devoted to B–N based chemical hydrides as potential hydrogen storage materials because of their high theoretical hydrogen capacity.^{1–3} For instance, ammonia borane (AB), with a high H-capacity of 19.6 wt%, is a typical B–N based hydride for chemical hydrogen storage.¹ However, upon decomposition of AB, accompanied volatile compounds of ammonia, diborane, and borazine are evolved, which lead to a reduction of dehydrogenation capacity and are fatal for fuel cell applications.^{1,4} Many different approaches have been adopted to facilitate hydrogen release from AB during the last decade.^{5–10} Recent studies show that the substitution of H atoms in the NH_3 unit of AB by alkali metals with the formation of single or double metal amidoborane (MAB) is an effective way to improve the dehydrogenation properties of AB in terms of the reduced H_2 release temperatures, accelerated H_2 release kinetics, and minimized borazine evolved.^{5,6,11–17}

Ammine metal borohydrides (AMBs), which show favourable hydrogen storage properties competitive with ammonia borane, have been developed recently as promising materials for hydrogen storage.^{18–31} However, many of these composites suffer from the release of undesirable gas of ammonia during

dehydrogenation. Further experimental results show that the purity of gas released and dehydrogenation temperature of AMBs can be improved by using double-cation substitutions approach and tuning BH_4/NH_3 ration.^{15,24,32,33} The experimental and theoretic studies indicate that ammonia is weakly bound to the metal cations with low electronegativity (<1.2) in AMBs, therefore tend to release ammonia at low temperature.^{32,34} Although these studies have provided valuable insight for understanding the decomposition processes of single metal cation AMBs, the results may not be applicable to double cations AMBs. For instance, $\text{Mg}(\text{BH}_4)_2 \cdot 2\text{NH}_3$ (with electronegativity of 1.31 for Mg cation) mainly release hydrogen along with a small amount of ammonia.²³ The incorporation of LiBH_4 (with low electronegativity of 0.98 for Li cation) and $\text{Mg}(\text{BH}_4)_2 \cdot 2\text{NH}_3$ with the formation of double cations ammine borohydride, $\text{LiMg}(\text{BH}_4)_3 \cdot 2\text{NH}_3$ results in improving the purity of gas released compared to $\text{Mg}(\text{BH}_4)_2 \cdot 2\text{NH}_3$.³⁵ Further improved dehydrogenation of ammine magnesium borohydride by tuning the NH_3/BH_4 ratios and combining $\text{Mg}(\text{BH}_4)_2 \cdot 2\text{NH}_3$ with MgH_2 and NaAlH_4 were reported.^{36–39}

The mixed-cation strategy offers a promising route toward tuneable dehydrogenation of ammine metal borohydrides, however, a detail study of the dehydrogenation mechanism is still needed for further improving their dehydrogenation performance. Herein, we presented a comparison study of the electronic structure and dehydrogenation mechanisms of $\text{Mg}(\text{BH}_4)_2 \cdot 2\text{NH}_3$ and $\text{LiMg}(\text{BH}_4)_3 \cdot 2\text{NH}_3$ by density functional theory (DFT) calculation.

^aDepartment of Physics, School of Science, Jimei University, Xiamen, 361021, China. E-mail: phyzwd@jmu.edu.cn

^bDepartment of Materials Science, Fudan University, Shanghai 200433, China. E-mail: yuxuebin@fudan.edu.cn

^{*}Institute for Superconducting and Electronic Materials, University of Wollongong, North Wollongong, NSW, Australia



Computational method

$\text{Mg}(\text{BH}_4)_2 \cdot 2\text{NH}_3$ crystallizes in the orthorhombic structure with space group of $Pcab$ and lattice parameters of $a = 17.4872(4)$ Å, $b = 9.4132(2)$ Å, $c = 8.7304(2)$ Å.²³ $\text{LiMg}(\text{BH}_4)_3 \cdot 2\text{NH}_3$ has a hexagonal structure with space group $P6_3$ and lattice constants of $a = b = 8.0002(1)$ Å and $c = 8.3944$ Å.³⁵ The geometric structures were optimized by DFT calculation as implemented in MedeA@VASP code.⁴⁰ To describe the weak van der Waals $\text{H}^+ \cdots \text{H}^-$ dihydrogen bonds, the optB86b-vdW functional^{41–43} was adopted for geometric optimization. Plane waves with kinetic energy cutoff of 500 eV were used. The generalized gradient approximation (GGA) of Perdew–Burke–Ernzerhof (PBE) was adapted to treat the exchange and correlation of electronics.^{44,45} The projector-augmented wave (PAW) approach was used to describe the electron-ion interactions⁴⁶ with 1s2s2p of Li, s2p1 of B, s2p3 of N, s2p0 of Mg as the explicit valence electrons. The Brillouin zones were sampled by Monkhorst–Pack k -point meshes⁴⁷ with meshes points spacing less than 0.05 per Å for both $\text{Mg}(\text{BH}_4)_2 \cdot 2\text{NH}_3$ and $\text{LiMg}(\text{BH}_4)_3 \cdot 2\text{NH}_3$. Structural relaxations of atomic positions were carried out until the total energies and residual forces were less than 1.0×10^{-5} eV and $0.02 \text{ eV } \text{Å}^{-1}$, respectively. For the calculation of NH_3 vacancy formation energies and H_2 formation energies, $1 \times 2 \times 2$ supercells of $\text{Mg}(\text{BH}_4)_2 \cdot 2\text{NH}_3$ and $2 \times 2 \times 2$ supercells of $\text{LiMg}(\text{BH}_4)_3 \cdot 2\text{NH}_3$ were used. Our tests showed that the used of $1 \times 2 \times 2$ supercells of $\text{Mg}(\text{BH}_4)_2 \cdot 2\text{NH}_3$ and $2 \times 2 \times 2$ supercells of $\text{LiMg}(\text{BH}_4)_3 \cdot 2\text{NH}_3$ with k -point mesh spacing less than 0.05 per Å yield energies that converged within $0.01 \text{ eV (f.u.)}^{-1}$. The NH_3 diffusion barriers and H_2 formation barriers were estimated by using climbing image nudged elastic band (CI-NEB) method.^{48,49}

The NH_3 vacancy formation energy was estimated using the following equation:

$$E_c = E_{\text{total}} - E(\text{AMBs-NH}_3) - E(\text{NH}_3)$$

where E_{total} is the total energy of the AMBs supercells; $E(\text{NH}_3)$ represents the energy of isolate NH_3 molecule; $E(\text{AMBs-NH}_3)$ is

the total energy of the AMBs supercells after NH_3 molecules are removed. The positive energy of E_c indicates that the creation of NH_3 vacancy is an endothermic process; while the negative energy of E_c indicates that the creation of NH_3 vacancy is an exothermic process.

The concentration of ammonia vacancy in $\text{Mg}(\text{BH}_4)_2 \cdot 2\text{NH}_3$ and $\text{LiMg}(\text{BH}_4)_3 \cdot 2\text{NH}_3$ could be estimated by the following equation⁵⁰

$$c = N_{\text{sites}} N_{\text{config}} \exp(E_c/kT)$$

where E_c is the formation energy of NH_3 vacancy; N_{sites} represents the number of sites that the defect can be incorporated; N_{config} is the number of configurations per site in which the vacancy can be formed; k and T represent Boltzmann constant and temperature, respectively.

Results and discussion

Electronic structure

The electron localization function (ELF) and charge transfer between the H, N, B atoms and metal cations (Li and Mg) were analysed to understand the bonding characters of $\text{Mg}(\text{BH}_4)_2 \cdot 2\text{NH}_3$ and $\text{LiMg}(\text{BH}_4)_3 \cdot 2\text{NH}_3$. The H atoms bond to N atom and B atom are represent as (N)H and (B)H, respectively. As shown in Fig. 1, the calculated ELF shows the covalent bonding of N–H and B–H. Although the Mg–H bonds are mainly ionic, the distorted ELF isosurfaces around (B)H, (N)H and Mg indicate partial covalent bond feature of Mg–H. The low ELF value around Li indicates the essentially ionic bonding character of Li–H. Table 1 shows the Bader charges of (B)H, N(H), N, B and Mg for $\text{Mg}(\text{BH}_4)_2 \cdot 2\text{NH}_3$ are $-0.58/-0.64$, 0.44 , -1.30 , 1.59 and 1.65 , respectively. The Bader charge of Li is 0.90 for $\text{LiMg}(\text{BH}_4)_3 \cdot 2\text{NH}_3$, indicates a strong ionization of the Li cation. Hence, Li cation transfers most of its 2s electron to neighbouring BH_4 unit, similar to that of LiBH_4 . Compared to $\text{Mg}(\text{BH}_4)_2 \cdot 2\text{NH}_3$, the incorporation of LiBH_4 with the formation of $\text{LiMg}(\text{BH}_4)_3 \cdot 2\text{NH}_3$ barely affects the charge distribution of H

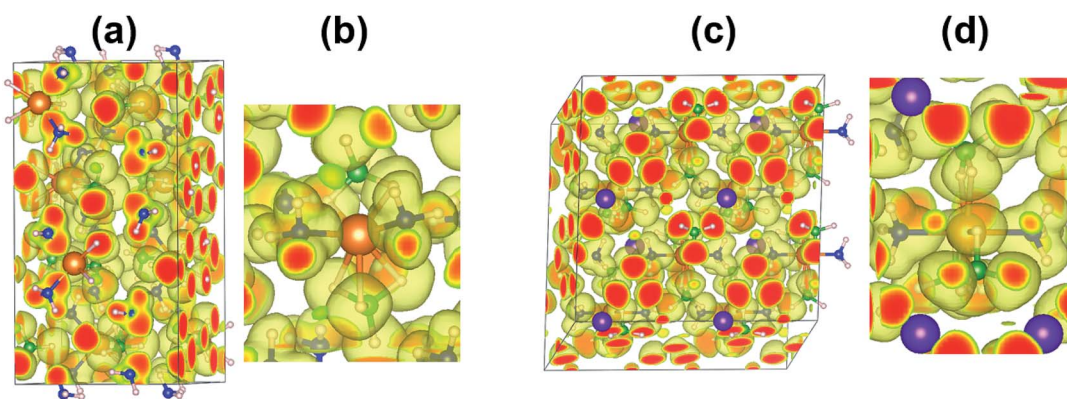


Fig. 1 The calculated electron localization function (ELF) for (a) $\text{Mg}(\text{BH}_4)_2 \cdot 2\text{NH}_3$ and (c) $\text{LiMg}(\text{BH}_4)_3 \cdot 2\text{NH}_3$ plotted as yellow-colored transparent isosurfaces at a level of 0.6; (b) and (d) present zoomed-in view showing more details for $\text{Mg}(\text{BH}_4)_2 \cdot 2\text{NH}_3$ and $\text{LiMg}(\text{BH}_4)_3 \cdot 2\text{NH}_3$, respectively. The green, pink, orange, purple and blue colors represent B, H, Mg, Li and N atoms, respectively.



Table 1 Bader charge of $\text{Mg}(\text{BH}_4)_2 \cdot 2\text{NH}_3$ and $\text{LiMg}(\text{BH}_4)_3 \cdot 2\text{NH}_3$

Atom	Bader charge	
	$\text{Mg}(\text{BH}_4)_2 \cdot 2\text{NH}_3$	$\text{LiMg}(\text{BH}_4)_3 \cdot 2\text{NH}_3$
Li	—	0.90
Mg	1.65	1.64
B	1.59	1.67
N	−1.30	−1.32/−1.34
(B)H	−0.58/−0.64	−0.63
(N)H	0.44	0.45

and Mg. The Bader charge of B is slightly increased and Bader charge of N is slightly decreased in $\text{LiMg}(\text{BH}_4)_3 \cdot 2\text{NH}_3$.

Ammonia vacancy formation energies and diffusion barriers

As demonstrated by previous report, $\text{Mg}(\text{BH}_4)_2 \cdot 2\text{NH}_3$ started to release hydrogen at temperature around 120 °C, with a maximum hydrogen release rate at 205 °C.²³ A small amount of NH_3 was released along with hydrogen evolution from $\text{Mg}(\text{BH}_4)_2 \cdot 2\text{NH}_3$. The $\text{LiMg}(\text{BH}_4)_3 \cdot 2\text{NH}_3$ shows dehydrogenation performance comparable to that of $\text{Mg}(\text{BH}_4)_2 \cdot 2\text{NH}_3$, with dehydrogenation peak located at 221 °C.³⁵ In addition, incorporation of LiBH_4 with $\text{Mg}(\text{BH}_4)_2 \cdot 2\text{NH}_3$ suppresses ammonia release.

The formation and transport properties of NH_3 vacancy are crucial to the thermodynamics and kinetics of ammonia release from AMBs. To understand the microscopic mechanisms behind the release of ammonia, the formation and diffusivity of NH_3 were studied. The NH_3 vacancy was created by directly removed a NH_3 unit from $\text{Mg}(\text{BH}_4)_2 \cdot 2\text{NH}_3$ and $\text{LiMg}(\text{BH}_4)_3 \cdot 2\text{NH}_3$.

As shown in Table 2, the calculated NH_3 removal energies are 1.81 and 1.97 eV for $\text{Mg}(\text{BH}_4)_2 \cdot 2\text{NH}_3$ and $\text{LiMg}(\text{BH}_4)_3 \cdot 2\text{NH}_3$, respectively. The relatively high NH_3 removal energies indicates that the formation of NH_3 vacancies are thermodynamics unfavourable at low temperature, resulting in low concentration of ammonia vacancy for those two composites. The high formation energy of NH_3 vacancies can attribute to the coordination bond of Mg–N and $\text{H}^+ \cdots \text{H}^-$ dihydrogen network.

In addition to the formation energies of NH_3 vacancies, the diffusivity of NH_3 vacancies is also importance for ammonia release. The diffusion paths were calculated by moving a NH_3 unit from a nearby lattice site into the vacancy. The diffusion barrier is defined as the energy difference between the saddle point and the ground state. The activation energy (Q) for self-diffusion of ammonia can be obtained by combining the

Table 2 Calculated NH_3 vacancy formation energies (E_c), diffusion barriers (E_b) and activation energies ($Q = E_b + E_c$) for $\text{Mg}(\text{BH}_4)_2 \cdot 2\text{NH}_3$ and $\text{LiMg}(\text{BH}_4)_3 \cdot 2\text{NH}_3$

	E_c (eV)	E_b (eV)	Q (eV)
$\text{Mg}(\text{BH}_4)_2 \cdot 2\text{NH}_3$	1.81	0.26	2.07
$\text{LiMg}(\text{BH}_4)_3 \cdot 2\text{NH}_3$	1.97	1.31	3.28

calculated vacancy formation energy with the diffusion barrier. As summarized in Fig. 2 and Table 2, for $\text{Mg}(\text{BH}_4)_2 \cdot 2\text{NH}_3$, the calculated energy barrier and activation energy of ammonia diffusion are 0.26 and 2.07 eV, respectively. It should be noted that the NH_3 diffusion barrier is relatively low, the formation energy of NH_3 vacancy is the dominate term in the activation energy for ammonia diffusion. The relatively high formation energy would result in low concentration of NH_3 vacancy, which limit its transport in $\text{Mg}(\text{BH}_4)_2 \cdot 2\text{NH}_3$. This is in agreement with previous report that only a small amount of NH_3 was released during decomposition of $\text{Mg}(\text{BH}_4)_2 \cdot 2\text{NH}_3$.²³

The calculated ammonia vacancy diffusion barrier and activation energy of $\text{LiMg}(\text{BH}_4)_3 \cdot 2\text{NH}_3$ are 1.31 and 3.28 eV, respectively. Compared to that of $\text{Mg}(\text{BH}_4)_2 \cdot 2\text{NH}_3$, the relatively high ammonia diffusion barrier and activation energy indicate that low concentration and mobility of ammonia vacancy in $\text{LiMg}(\text{BH}_4)_3 \cdot 2\text{NH}_3$, in inconsistent with experimental results that the dehydrogenation purity of $\text{Mg}(\text{BH}_4)_2 \cdot 2\text{NH}_3$ can be improved by introducing LiBH_4 with the formation of $\text{LiMg}(\text{BH}_4)_3 \cdot 2\text{NH}_3$.³⁵

Hydrogen formation energies and barriers

Our previous studies suggest that the initial dehydrogenation of AMBs is achieved by combination of H atoms from NH_3 and H atoms from BH_4 groups.^{51,52} Therefore, H_2 formation energies were calculated by moving one (N)H and one (B)H atom away from host N or B atom to form a hydrogen molecule with H–H distance of 0.74 Å in the supercell of AMBs. The geometry optimization was first performed by fixed the H_2 positions and relaxed the rest of the atoms, following by full relaxed all of the atoms in the supercell. In agreement with our previous studies, the formation of H_2 molecules lead to significant rearrangement of the surrounding lattice, which may result in over-estimated the hydrogen formation energies. In addition, both $\text{Mg}(\text{BH}_4)_2 \cdot 2\text{NH}_3$ and $\text{LiMg}(\text{BH}_4)_3 \cdot 2\text{NH}_3$ started to release hydrogen at temperature higher than their melting point. In other word, the crystal structure of $\text{Mg}(\text{BH}_4)_2 \cdot 2\text{NH}_3$ and $\text{LiMg}(\text{BH}_4)_3 \cdot 2\text{NH}_3$ disappeared before hydrogen evolved. Therefore, we further calculated the hydrogen formation energies by using the molecule model in which two formula units of $\text{Mg}(\text{BH}_4)_2 \cdot 2\text{NH}_3$ and $\text{LiMg}(\text{BH}_4)_3 \cdot 2\text{NH}_3$ were placed in a cubic cell with lattice parameter of 20 Å.

As shown in Table 3, the calculated hydrogen formation energies by using supercell of AMBs are 0.84 and 1.22 eV for $\text{Mg}(\text{BH}_4)_2 \cdot 2\text{NH}_3$ and $\text{LiMg}(\text{BH}_4)_3 \cdot 2\text{NH}_3$, respectively. In consistent with our previous theoretical study, the dissociation of H_2 results in dramatic movement of around atoms.⁵¹ The hydrogen formation energies calculated by molecule model are −0.11 and 0.08 eV for $\text{Mg}(\text{BH}_4)_2 \cdot 2\text{NH}_3$ and $\text{LiMg}(\text{BH}_4)_3 \cdot 2\text{NH}_3$, respectively. The combination of the (N)H and (B)H results in rearrangement of the surrounding atoms, similar with our previous report.⁵¹ The NH_2 and BH_3 units reoriented and BH_3 units moved toward NH_2 to form $\text{NH}_2\text{--BH}_3$ complexes. The N–B distances reduce to 1.58 Å, indicating the formation of N–B bond during dehydrogenation, in agreement with experimental observation.^{14,35} However, the lengths of Li–



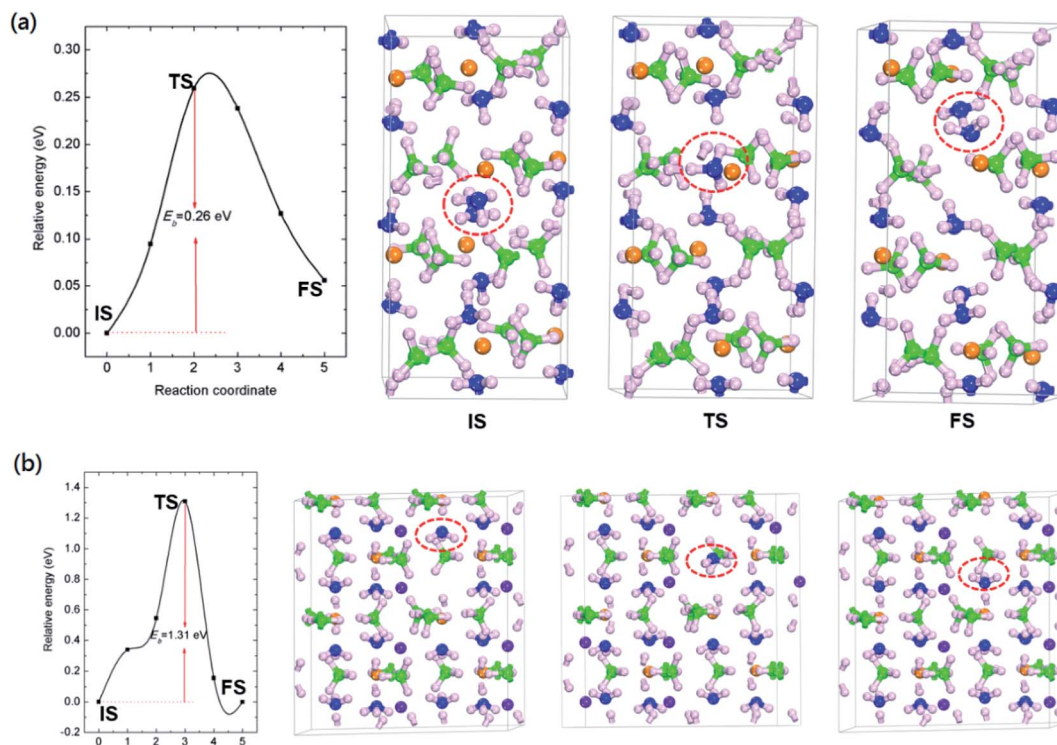


Fig. 2 The calculated energetic profiles, initial (IS), transition (TS) and final (FS) geometric structure of NH_3 diffusion for (a) $\text{Mg}(\text{BH}_4)_2 \cdot 2\text{NH}_3$ and (b) $\text{LiMg}(\text{BH}_4)_3 \cdot 2\text{NH}_3$. E_b represents the calculated energy barrier. The green, pink, orange, purple and blue colors represent B, H, Mg, Li and N atoms, respectively.

Table 3 Formation energies of H_2 release via (N)H and (B)H combination by using crystal model ($E_{\text{H}_2\text{-C}}$) and molecule model ($E_{\text{H}_2\text{-M}}$)

	$E_{\text{H}_2\text{-C}}$ (eV)	$E_{\text{H}_2\text{-M}}$ (eV)
$\text{Mg}(\text{BH}_4)_2 \cdot 2\text{NH}_3$	0.84	-0.11
$\text{LiMg}(\text{BH}_4)_3 \cdot 2\text{NH}_3$	1.22	0.08

N, Mg–N, B–H and N–H bonds keep almost the same after structural rearrangements.

The low H_2 formation energies of $\text{Mg}(\text{BH}_4)_2 \cdot 2\text{NH}_3$ and $\text{LiMg}(\text{BH}_4)_3 \cdot 2\text{NH}_3$ suggest that the formation of hydrogen is thermodynamic favourable at low temperature. Therefore, the energy barrier of H_2 formation is the key of those two composites release hydrogen at temperature above 100°C .

We further calculated the energy barriers of H_2 formation and the results were summarized in Fig. 3. The calculated energy barrier of H_2 formation from $\text{Mg}(\text{BH}_4)_2 \cdot 2\text{NH}_3$ is 2.20 eV. The transition geometric structure of hydrogen release from $\text{Mg}(\text{BH}_4)_2 \cdot 2\text{NH}_3$ (Fig. 3(a)) shows the broken of B–H and N–H bonds with the formation of H_2 molecule. The H_2 molecule is located between NH_2 and BH_3 units with $\text{H}_2\text{-NH}_2$ and $\text{H}_2\text{-BH}_3$ distances of 2.47 and 2.31 Å, respectively. Meanwhile, the NH_2 unit move toward Mg cation and lead to slightly reduce the Mg–N distance from 2.16 to 1.95 Å. The calculated hydrogen formation energy barrier of $\text{LiMg}(\text{BH}_4)_3 \cdot 2\text{NH}_3$ is 2.55 eV, which is 0.35 eV higher than that of $\text{Mg}(\text{BH}_4)_2 \cdot 2\text{NH}_3$. Previous experimental results show dehydrogenation peak of 205°C and

221°C for $\text{Mg}(\text{BH}_4)_2 \cdot 2\text{NH}_3$ and $\text{LiMg}(\text{BH}_4)_3 \cdot 2\text{NH}_3$, respectively.^{23,35} The relatively high dehydrogenation peak of $\text{LiMg}(\text{BH}_4)_3 \cdot 2\text{NH}_3$ can be attributed to the high hydrogen formation barrier. The transition geometric structure of hydrogen release from $\text{LiMg}(\text{BH}_4)_3 \cdot 2\text{NH}_3$ is similar to that of $\text{Mg}(\text{BH}_4)_2 \cdot 2\text{NH}_3$. The H_2 molecule is located between NH_2 and BH_3 unit. The $\text{H}_2\text{-NH}_2$ distance in transition structure of $\text{LiMg}(\text{BH}_4)_3 \cdot 2\text{NH}_3$ is 2.24 Å, which is 0.23 Å shorter than that in $\text{Mg}(\text{BH}_4)_2 \cdot 2\text{NH}_3$. And the $\text{H}_2\text{-BH}_3$ distance in transition structure of $\text{LiMg}(\text{BH}_4)_3 \cdot 2\text{NH}_3$ is 2.11 Å, which is 0.20 Å shorter than that in $\text{Mg}(\text{BH}_4)_2 \cdot 2\text{NH}_3$. In addition, the NH_2 unit shortening its distance to the Mg cation from 2.19 to 1.95 Å, similar to that of $\text{Mg}(\text{BH}_4)_2 \cdot 2\text{NH}_3$.

Although the above calculations show a low NH_3 diffusion barrier for $\text{Mg}(\text{BH}_4)_2 \cdot 2\text{NH}_3$, the formation energy of NH_3 vacancy is relatively high, which results in low concentration of NH_3 vacancy in $\text{Mg}(\text{BH}_4)_2 \cdot 2\text{NH}_3$. Therefore, the $\text{Mg}(\text{BH}_4)_2 \cdot 2\text{NH}_3$ mainly releases hydrogen accompany with a small amount of ammonia during decomposition. In contrast to that of $\text{Mg}(\text{BH}_4)_2 \cdot 2\text{NH}_3$, $\text{LiMg}(\text{BH}_4)_3 \cdot 2\text{NH}_3$ shows relatively high formation energy and diffusion barrier of NH_3 vacancy, which limit both the concentration and transport of ammonia, therefore improve the dehydrogenation purity. The calculated hydrogen formation barrier of $\text{LiMg}(\text{BH}_4)_3 \cdot 2\text{NH}_3$ is slightly higher than that of $\text{Mg}(\text{BH}_4)_2 \cdot 2\text{NH}_3$, therefore incorporation of LiBH_4 with $\text{Mg}(\text{BH}_4)_2 \cdot 2\text{NH}_3$ may not decrease the dehydrogenation temperature.



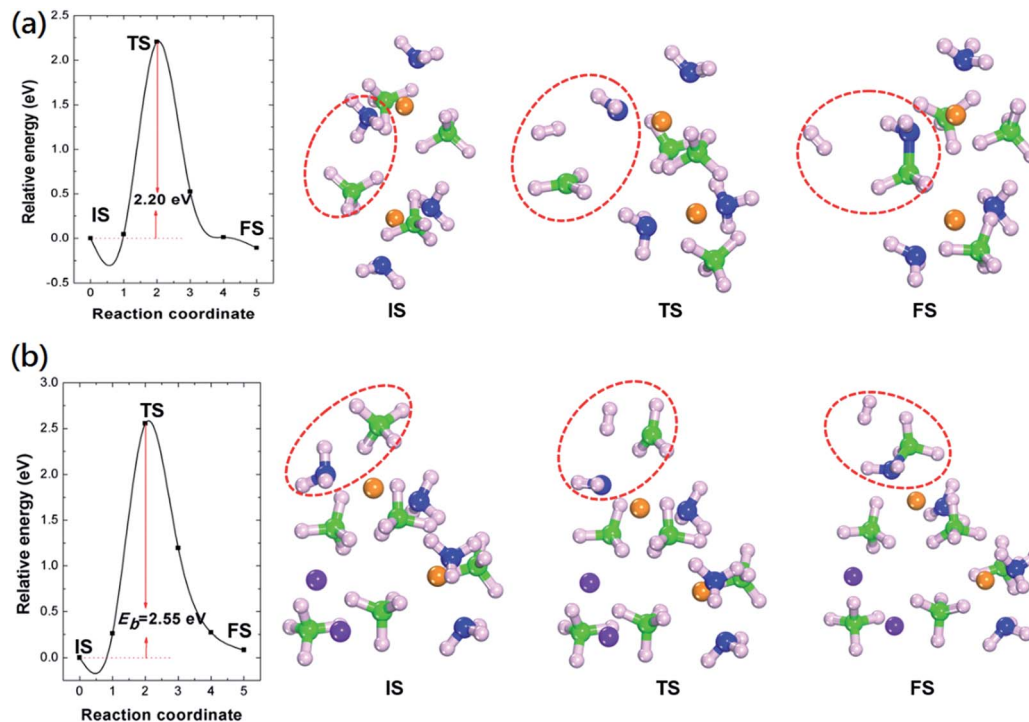


Fig. 3 The calculated energetic profiles, initial (IS), transition (TS) and final (FS) geometric structure of H₂ formation for (a) Mg(BH₄)₂·2NH₃ and (b) LiMg(BH₄)₃·2NH₃. E_b represents the calculated energy barrier. The green, pink, orange, purple and blue colours represent B, H, Mg, Li and N atoms, respectively.

Conclusions

First-principles calculations based on density functional theory were carried out to investigate the decomposition mechanisms of Mg(BH₄)₂·2NH₃ and LiMg(BH₄)₃·2NH₃. The electronic structure analysis indicates that Mg–H interaction in those two composites are mainly ionic with partial covalent bond feature. The incorporation of LiBH₄ and Mg(BH₄)₂·2NH₃ with the formation of LiMg(BH₄)₃·2NH₃ barely affects the charge distribution of H and Mg. The Bader charge of B is slightly increased and Bader charge of N decreased due to the incorporation of LiBH₄. Although the NH₃ diffusion barrier for Mg(BH₄)₂·2NH₃ is low, the relatively high formation energy of NH₃ vacancy lead to low concentration of NH₃ vacancy and limit its transportation, in agreement with experimental results that Mg(BH₄)₂·2NH₃ mainly releases hydrogen along with a small amount of ammonia. The LiMg(BH₄)₃·2NH₃ shows relatively high ammonia vacancy formation energy and diffusion barrier, which suppress ammonia release compared to Mg(BH₄)₂·2NH₃. The incorporation of LiBH₄ and Mg(BH₄)₂·2NH₃ does not decrease the hydrogen formation barriers, instead slightly increase the hydrogen formation barriers of LiMg(BH₄)₃·2NH₃, in agreement with experimental results that LiMg(BH₄)₃·2NH₃ shows a dehydrogenation peak slightly higher than that of Mg(BH₄)₂·2NH₃.

Acknowledgements

This work is supported by the National Science Fund for Distinguished Young Scholars (51625102), National Natural Science

Foundation of China (51601068, 11605073) and Natural Science Foundation of Fujian Province (2016J05129, 2017J05009).

Notes and references

- 1 A. Staubitz, A. P. M. Robertson and I. Manners, *Chem. Rev.*, 2010, **110**, 4079–4124.
- 2 C. W. Hamilton, R. T. Baker, A. Staubitz and I. Manners, *Chem. Soc. Rev.*, 2009, **38**, 279–293.
- 3 Z. Xiong, C. K. Yong, G. Wu, P. Chen, W. Shaw, A. Karkamkar, T. Autrey, M. O. Jones, S. R. Johnson and P. P. Edwards, *Nat. Mater.*, 2008, **7**, 138–141.
- 4 T. B. Marder, *Angew. Chem., Int. Ed.*, 2007, **46**, 8116–8118.
- 5 L. Li, X. Yao, C. Sun, A. Du, L. Cheng, Z. Zhu, C. Yu, J. Zou, S. C. Smith and P. Wang, *Adv. Funct. Mater.*, 2009, **19**, 265–271.
- 6 X. Kang, Z. Fang, L. Kong, H. Cheng, X. Yao, G. Lu and P. Wang, *Adv. Mater.*, 2008, **20**, 2756–2759.
- 7 A. Paul and C. B. Musgrave, *Angew. Chem., Int. Ed.*, 2007, **119**, 8301–8304.
- 8 W. R. H. Wright, E. R. Berkeley, L. Alden, R. T. Baker and L. G. Sneddon, *Chem. Commun.*, 2011, **47**, 3177–3179.
- 9 X. Kang, J. Luo, Q. Zhang and P. Wang, *Dalton Trans.*, 2011, **40**, 3799–3801.
- 10 B. Meredig and C. Wolverton, *Nat. Mater.*, 2012, **12**, 123–127.
- 11 A. Karkamkar, C. Aardahl and T. Autrey, *Mater. Matters*, 2007, **2**, 6–9.
- 12 H. Wu, W. Zhou, F. E. Pinkerton, M. S. Meyer, Q. Yao, S. Gadipelli, T. J. Udovic, T. Yildirim and J. J. Rush, *Chem. Commun.*, 2011, **47**, 4102–4104.



- 13 J. Luo, X. Kang and P. Wang, *Energy Environ. Sci.*, 2013, **6**, 1018–1025.
- 14 Y. S. Chua, H. Wu, W. Zhou, T. J. Udovic, G. Wu, Z. Xiong, M. W. Wong and P. Chen, *Inorg. Chem.*, 2012, **51**, 1599–1603.
- 15 G. Xia, Y. Tan, X. Chen, Z. Guo, H. Liu and X. Yu, *J. Mater. Chem. A*, 2013, **1**, 1810–1820.
- 16 J. Spielmann, G. Jansen, H. Bandmann and S. Harder, *Angew. Chem., Int. Ed.*, 2008, **120**, 6386–6391.
- 17 X. Chen, Y.-J. Zhao and X. Yu, *Phys. Chem. Chem. Phys.*, 2013, **15**, 893–900.
- 18 Y. H. Guo, X. B. Yu, W. W. Sun, D. L. Sun and W. N. Yang, *Angew. Chem., Int. Ed.*, 2011, **123**, 1119–1123.
- 19 Y. H. Guo, G. L. Xia, Y. Zhu, L. Gao and X. B. Yu, *Chem. Commun.*, 2010, **46**, 2599–2601.
- 20 P. A. Chater, W. I. David, S. R. Johnson, P. P. Edwards and P. A. Anderson, *Chem. Commun.*, 2006, 2439–2441.
- 21 H. Chu, G. Wu, Z. Xiong, J. Guo, T. He and P. Chen, *Chem. Mater.*, 2010, **22**, 6021–6028.
- 22 F. Yuan, Q. F. Gu, X. W. Chen, Y. B. Tan, Y. H. Guo and X. B. Yu, *Chem. Mater.*, 2012, **24**, 3370–3379.
- 23 G. Soloveichik, J. H. Her, P. W. Stephens, Y. Gao, J. Rijssenbeek, M. Andrus and J. C. Zhao, *Inorg. Chem.*, 2008, **47**, 4290–4298.
- 24 Y. H. Guo, H. Wu, W. Zhou and X. B. Yu, *J. Am. Chem. Soc.*, 2011, **133**, 4690–4693.
- 25 L. H. Jepsen, M. B. Ley, R. Cerný, Y. Lee, Y. W. Cho, D. B. Ravnsbaek, F. Besenbacher, J. Skibsted and T. R. Jensen, *Inorg. Chem.*, 2015, **54**, 7402–7414.
- 26 K. Wang, J. Zhang and X. Lang, *Phys. Chem. Chem. Phys.*, 2016, **18**, 7015–7018.
- 27 J. M. Huang, L. Z. Ouyang, Q. F. Gu, X. B. Yu and M. Zhu, *Chem.–Eur. J.*, 2015, **21**, 14931–14936.
- 28 J. Huang, Y. Tan, J. Su, Q. Gu, R. Cerný, L. Ouyang, D. Sun, X. Yu and M. Zhu, *Chem. Commun.*, 2015, **51**, 2794–2797.
- 29 Y. J. Yang, Y. F. Liu, Y. Li, M. X. Gao and H. G. Pan, *J. Mater. Chem. A*, 2015, **3**, 570–578.
- 30 Y. Li, Y. F. Liu, X. Zhang, D. Zhou, Y. H. Lu, M. X. Gao and H. G. Pan, *J. Mater. Chem. A*, 2016, **4**, 8366–8373.
- 31 Y. J. Yang, Y. F. Liu, Y. Li, X. Zhang, M. X. Gao and H. G. Pan, *J. Mater. Chem. A*, 2015, **3**, 11057–11065.
- 32 Z. Tang, Y. Tan, H. Wu, Q. Gu, W. Zhou, C. M. Jensen and X. Yu, *Acta Mater.*, 2013, **61**, 4787–4796.
- 33 A. Emdadi, S. Demir, Y. Kışlak and A. Tekin, *J. Phys. Chem. C*, 2016, **120**, 13340–13350.
- 34 E. Welchman and T. Thonhauser, *J. Mater. Chem. A*, 2017, **5**, 4084–4092.
- 35 W. W. Sun, X. W. Chen, Q. F. Gu, K. S. Wallwork, Y. B. Tan, Z. W. Tang and X. B. Yu, *Chem.–Eur. J.*, 2012, **18**, 6825–6834.
- 36 Y. Yang, Y. Liu, Y. Li, M. Gao and H. Pan, *Chem.–Asian J.*, 2013, **8**, 476–481.
- 37 Y. Yang, Y. Liu, H. Wu, W. Zhou, M. Gao and H. Pan, *Phys. Chem. Chem. Phys.*, 2013, **16**, 135–143.
- 38 Y. Yang, Y. Liu, Y. Zhang, Y. Li, M. Gao and H. Pan, *J. Alloys Compd.*, 2014, **585**, 674–680.
- 39 Y. Li, Y. Liu, X. Zhang, Y. Yang, M. Gao and H. Pan, *Int. J. Hydrogen Energy*, 2016, **41**, 2788–2796.
- 40 G. Kresse and J. Furthmüller, *Phys. Rev. B: Condens. Matter Mater. Phys.*, 1996, **54**, 11169.
- 41 J. Klimes, D. R. Bowler and A. Michaelides, *Phys. Rev. B: Condens. Matter Mater. Phys.*, 2011, **83**, 195131.
- 42 J. Klimes, D. R. Bowler and A. Michaelides, *J. Phys.: Condens. Matter*, 2009, **22**, 022201.
- 43 M. Dion, H. Rydberg, E. Schroder, D. C. Langreth and B. I. Lundqvist, *Phys. Rev. Lett.*, 2004, **92**, 246401.
- 44 J. P. Perdew, K. Burke and M. Ernzerhof, *Phys. Rev. Lett.*, 1996, **77**, 3865–3868.
- 45 J. P. Perdew, K. Burke and Y. Wang, *Phys. Rev. B: Condens. Matter Mater. Phys.*, 1996, **54**, 16533–16539.
- 46 P. E. Blöchl, *Phys. Rev. B: Condens. Matter Mater. Phys.*, 1994, **50**, 17953.
- 47 H. J. Monkhorst and J. D. Pack, *Phys. Rev. B: Condens. Matter Mater. Phys.*, 1976, **13**, 5188–5192.
- 48 G. Henkelman, B. P. Uberuaga and H. Jónsson, *J. Chem. Phys.*, 2000, **113**, 9901–9904.
- 49 G. Henkelman and H. Jónsson, *J. Chem. Phys.*, 2000, **113**, 9978–9985.
- 50 C. G. van de Walle and J. Neugebauer, *J. Appl. Phys.*, 2004, **95**, 3851.
- 51 X. W. Chen and X. B. Yu, *J. Phys. Chem. C*, 2012, **116**, 11900–11906.
- 52 X. W. Chen, F. Yuan, Y. B. Tan, Z. W. Tang and X. B. Yu, *J. Phys. Chem. C*, 2012, **116**, 21162–21168.

